npg

ORIGINAL ARTICLE

Effects on tumor development and metastatic dissemination by the NKG2D lymphocyte receptor expressed on cancer cells

A El-Gazzar[1], X Cai[1], RS Reeves[1], Z Dai, A Caballero-Benitez, DL McDonald, J Vazquez, TA Gooley, GE Sale, T Spies and V Groh

The stimulatory NKG2D lymphocyte receptor together with its tumor-associated ligands enable the immune system to recognize and destroy cancer cells. However, with dynamic changes unfolding, cancers exploit NKG2D and its ligands for immune evasion and suppression. Recent findings have added yet another functional dimension, wherein cancer cells themselves co-opt NKG2D for their own benefit to complement the presence of its ligands for self-stimulation of parameters of tumorigenesis. Those findings are here extended to *in vivo* tumorigenicity testing by employing orthotopic xenotransplant breast cancer models in mice. Using human cancer lines with ectopic NKG2D expression and RNA interference (RNAi)-mediated protein depletion among other controls, we show that NKG2D self-stimulation has tumor-promoting capacity. NKG2D signals had no notable effects on cancer cell proliferation and survival but acted at the level of angiogenesis, thus promoting tumor growth, tumor cell intravasation and dissemination. NKG2D-mediated effects on tumor initiation may represent another factor in the observed overall enhancement of tumor development. Altogether, these results may have an impact on immunotherapy approaches, which currently do not account for such NKG2D effects in cancer patients and thus could be misdirected as underlying assumptions are incomplete.

INTRODUCTION

NKG2D is an activating lymphocyte receptor that has a prominent role in tumor immune surveillance owing to the tumor-associated expression of its ligands.[1] NKG2D is a type II transmembrane-anchored lectin-like receptor that is mainly present on natural killer (NK) cells and CD8 T cells.[2] It forms homodimers that gain stable surface expression and functional competence through assembly with four chains of the signaling adaptor protein DAP10.[2,3] Distinct from mice, there is no shortened human NKG2D variant that can also bind DAP12.[3] Upon ligation of NKG2D, DAP10 is phosphorylated at a cytoplasmic tail tyrosine-based motif and recruits either the p85 subunit of phosphoinositide 3-kinase (PI3K) or the growth factor receptor-bound protein 2, thereby activating protein kinase B (PKB/AKT) and mitogen-activated protein kinase (MAPK) signaling cascades.[4] These activities ultimately promote lymphocyte effector functions, proliferation and survival.

NKG2D interacts with multiple ligands that are distant relatives of major histocompatibility complex class I polypeptides but without their features linked to antigen presentation. Human NKG2D ligands include the major histocompatibility complex class I-related chains A and B (MICA and MICB) and six members of the structurally diverse UL16-binding proteins (ULBP1–ULBP6).[5,6] Typically, these ligands are either absent from the surface of most normal cells or are insufficient or ineffectively disposed to stimulate an immune response. However, they are prominently expressed in malignancies owing to their transcriptional induction by cellular stress responses, proliferation and signaling intermediates and checkpoint anomalies associated with oncogenic states.[7] With cancers, essentially all types have variable cell proportions expressing mainly MICA/B and at least one member of the ULBP ligand family.

In a conceptual twist, recent observations uncovered the expression of functionally competent NKG2D–DAP10 complexes on the surface of cancer cells themselves. Variable proportions of *ex vivo* tumor cells from breast, ovarian, prostate and colon cancers express NKG2D–DAP10, which upon ligand engagement or antibody crosslinking activate the oncogenic PI3K–AKT–mammalian target of rapamycin signaling axis and downstream effectors and trigger phosphorylation of ERK and JNK in MAPK cascades downstream of PI3K and growth factor receptor-bound protein 2, respectively.[8] Hence, cancer cells may co-opt the expression of NKG2D receptors to complement the presence of its ligands for self-stimulation of oncogenic signaling circuitries that can promote tumor growth and malignant dissemination. In fact, above-threshold expression of NKG2D–DAP10 in the ligand-bearing MCF-7 breast cancer line enhances cell cycle progression and bioenergetic metabolism.[8] Moreover, significant correlations have been established between percentages of cancer cells that are positive for surface NKG2D and tumor size or spread in an exploratory clinicopathologic association study of primary breast, ovarian, prostate and colon cancers.[8]

Despite this evidence, however, in the absence of an *in vivo* tumorigenicity model demonstrating pathophysiological significance, the proposed role of NKG2D as an oncoprotein has incomplete support. This study therefore aims at filling this void. Using ectopic NKG2D–DAP10 expression in classical orthotopic breast cancer line xenotransplants in mice, we show that ligand-mediated NKG2D self-stimulation has tumor-promoting capacity.

2

NKG2D signals had no notable effect on cancer cell proliferation and survival but acted at the level of angiogenesis, thus promoting tumor growth, tumor cell intravasation and dissemination. NKG2D-mediated effects on tumor initiation may represent another factor in the observed overall enhancement of tumor development.

RESULTS

Cancer cell NKG2D reduces latency and enhances tumor take in an orthotopic MCF-7 breast cancer xenotransplant model

In vitro evidence for functional significance of NKG2D in cancer cells has been obtained using the MCF-7 breast cancer line expressing the MICA/B, ULBP1 and ULBP3 ligands and its NKG2D–DAP10-transfected and NKG2D-depleted variants.[8] We therefore chose to test cancer cell NKG2D for in vivo tumorigenic effects in breast cancer models of primary and metastatic tumor progression in mice. Although MCF-7 cells are minimally invasive and estrogen-dependent, they are considered well suited for orthotopic xenograft models of tumor development and progression in immunodeficient mice.[9] We thus initiated our in vivo studies using the previously established NKG2D–DAP10 and mock control (MCF-7–TF and MCF-7–mock) transfectants.[8] Groups of each 14 estrogen-supplemented non-obese diabetic/severe combined immunodeficient mice received matrigel-supported unilateral axillary mammary fat pad injections of MCF-7–TF or MCF-7–mock cells. Tumor development was recorded weekly by external caliper. To allow for examination of NKG2D phenotypes and tumorigenesis over time, three mice in each group were killed at 4, 6 and 8 weeks post inoculation. The remaining mice were monitored for at least 13 weeks. Tumor latency and incidence were strikingly different between the two groups. By weeks 2 and 3, 9 and 11 out of the 14 MCF-7–TF mice, respectively, had developed measurable tumors, whereas only one out of 11 control animals had a measurable tumor mass by week 5 (Figure 1a). This effect was because of the ectopic expression of NKG2D as confirmed by comparison of the experimental data to those obtained from implants of MCF-7–TF cells with RNA interference (RNAi)-induced depletion of NKG2D (MCF-7–TF–RNAi) versus scrambled RNAi (scrRNAi) controls (MCF-7–TF–scrRNAi) (Figure 1b). As opposed to NKG2D-positive ex vivo cancer cells, most tumor lines have no or little NKG2D. In MCF-7 cells, endogenous NKG2D is scarce but nevertheless signaling-proficient.[8] The minimal expression of endogenous NKG2D was almost certainly accountable for the extended tumor latency observed with NKG2D-depleted MCF-7 (MCF-7–RNAi) cells as compared with the MCF-7–scrRNAi control, thus providing further support for a physiological role of this receptor and by infering its ligands in promoting tumor initiation (Figure 1c).

At first sight, comparisons of tumor volumes also suggested differences between experimental groups, with the MCF-7–TF tumor growth curve appearing steeper than that of the MCF-7–mock control tumors (Figure 1d). However, when tumor volumes were controlled for time of tumor appearance, those differences became minimal and eventually disappeared (Figure 1e). This disconnect between NKG2D-mediated effects on tumor latency and take, and tumor growth, was consistent with the loss of ectopic NKG2D expression on most (>90%) tumor cells in all of three MCF-7–TF-derived tumors tested on week 4 (Figure 2a). By week 6, surface NKG2D had further declined and was entirely lost by week 8. Thus, although NKG2D signals may have initiated cellular changes leading to enhancement of tumor initiation, we discarded the MCF-7 model as non-suitable for further studies of primary and metastatic tumorigenicity under persistent NKG2D signaling conditions as initially planned.
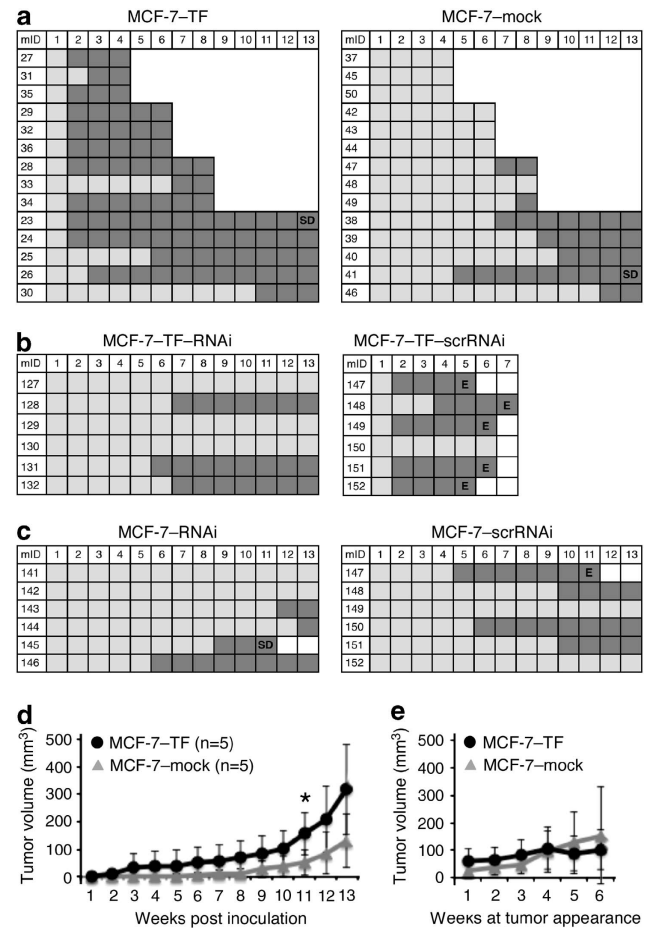
Figure 1. NKG2D effects on tumor latency, incidence and growth in the orthotopic MCF-7 xenotransplant model. (a–c) Graphic representations of tumor development over time measured in weekly intervals (top numbers) following implantation of the MCF-7 model lines. Left vertical numbers refer to mouse identifications (mID). Dark gray squares indicate presence of measurable tumor mass; light gray squares indicate absence of tumor mass. SD, spontaneous death, E, euthanasia. (a) Implanted MCF-7–TF cells develop tumors earlier and more frequently than MCF-7–mock control cells. The staircase representation reflects termination of each three mice per group at weeks 4, 6 and 8. Remaining mice were maintained for a minimum of 13 and a maximum of 14 weeks (see text). (b) Delayed appearance and reduced frequency of MCF-7–TF–RNAi tumors compared with MCF-7–TF–scrRNAi controls. (c) RNAi-mediated depletion of minimal endogenous NKG2D enhances latency of MCF-7–RNAi compared with MCF-7–scrRNAi tumors. (d) Graphic representations of MCF-7–TF and MCF-7–mock tumor volume averages and s.d.'s at the indicated weekly time intervals post-tumor cell inoculation. Data were derived from each five mice per group corresponding to those in (a) monitored for 13 or 14 weeks. Asterisk denotes $P < 0.05$. (e) Graphic representation of MCF-7–TF and MCF-7–mock tumor volume averages normalized to times of tumor appearance. Data were derived from the same mice studied in (d). Normalization of tumor volumes to times of tumor appearances affects group sizes at each weekly interval as follows: weeks 1–3, MCF-7–TF ($n = 5$) and MCF-7–mock ($n = 5$); week 4, MCF-7–TF ($n = 5$) and MCF-7–mock ($n = 4$); week 5, MCF-7–TF ($n = 4$) and MCF-7–mock ($n = 4$); week 6, MCF-7–TF ($n = 4$) and MCF-7–mock ($n = 3$).

Cancer cell NKG2D enhances tumor growth in an orthotopic SUM149PT breast cancer xenotransplant model

Similar to MCF-7, the SUM149PT breast cancer line, which expresses NKG2D ligands MICA/B and ULBP4, is widely used for in vivo mouse models addressing tumor growth and
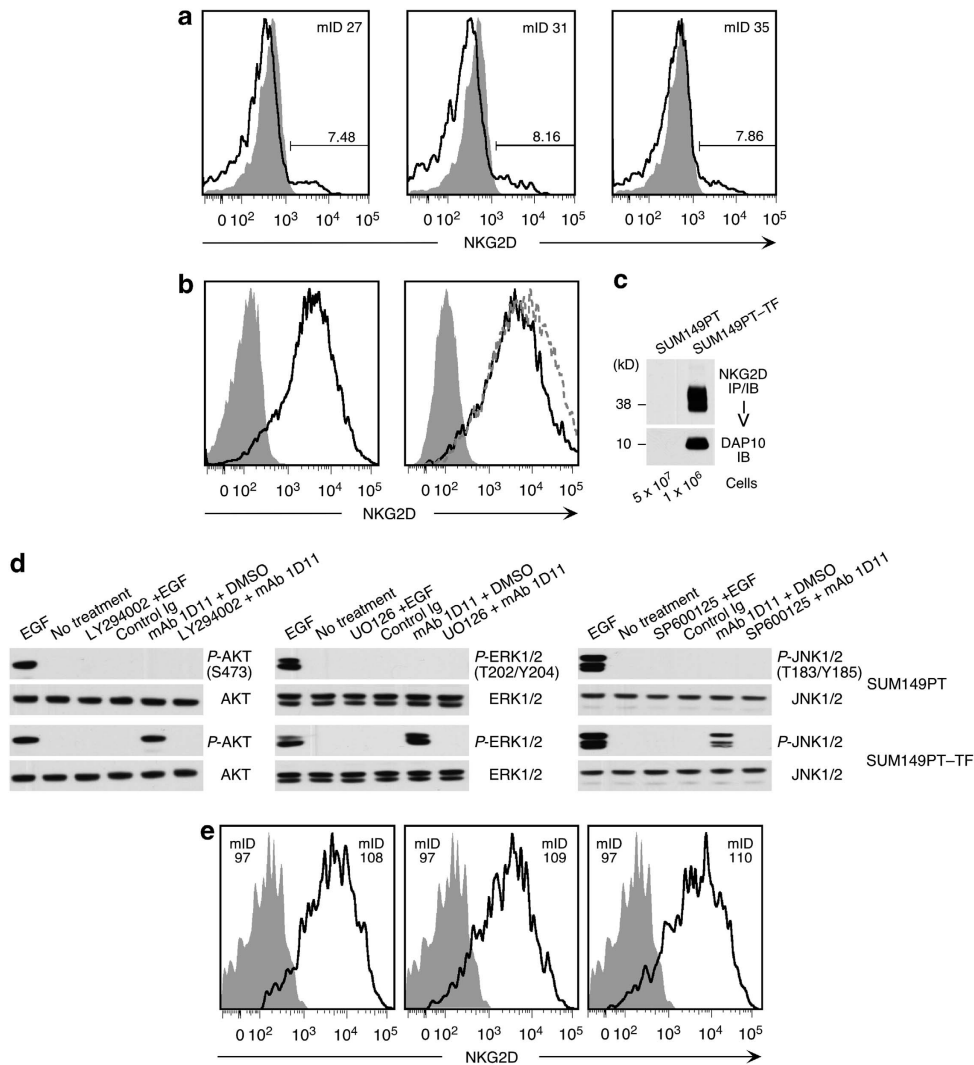
Figure 2. NKG2D expression on experimental cell lines and xenograft tumor cells and signaling proficiency. (**a**) Loss of ectopic NKG2D expression in MCF-7–TF xenotransplant tumors determined using cell suspension flow cytometry. Open profiles represent MCF-7–TF tumors harvested at week 4 post implantation (see Figure 1a). Shaded profiles represent the control MCF-7–mock line. mIDs are indicated in upper right corners. Numbers above bars indicate NKG2D-positive cells (in %). (**b**) Confirmation of NKG2D phenotypes of SUM149PT-derived model lines. Left histogram shows ectopic NKG2D expression on SUM149PT–TF cells (open profile) versus NKG2D-negative SUM149PT–mock cells (shaded profile). Right histogram displays NKG2D-positive SUM149PT–TF (open profile) and SUM149PT–TF–scrRNAi cells (open dotted line profile) versus NKG2D-negative SUM149PT–TF–RNAi cells (shaded profile). (**c**) Confirmation of NKG2D–DAP10 expression in SUM149PT–TF cells using immunoprecipitation (IP) with bead-coupled anti-NKG2D mAb 5C6 from lysate of 5×10^6 cells and sequential immunoblot (IB) probing for NKG2D and DAP10. We used 5×10^7 cells of the parental control SUM149PT line to rule out even minimal expression of NKG2D. (**d**) SUM149PT–TF but not SUM149PT cells are endowed with NKG2D–DAP10 signaling after desensitization and receptor crosslinking using mAb 1D11. Immunoblots were probed for phosphoproteins P-AKT (S473), P-ERK1/2 (T202/Y204) and P-JNK1/2 (T183/Y185). Total cellular AKT, ERK and JNK served as loading controls. Exposure to EGF provided for activation control. Pharmacological inhibitors were LY294002 (of PI3K), UO126 (of MEK/ERK) and SP600125 (of JNK). Dimethyl sulfoxide was included as solvent control. (**e**) Stable ectopic NKG2D expression in SUM149–TF xenotransplant tumors determined using cell suspension flow cytometry. Open profiles represent run 1 SUM149PT–TF tumors harvested at week 7 post implantation (see Figure 3a). Shaded profiles represent SUM149PT–mock tumor controls. All profiles were derived from GFP-positive tumor cells. mIDs in upper right corners refer to SUM149PT–TF xenotransplants. In left corners, mID 97 refers to a SUM149PT–mock-implanted mouse.

dissemination.[9] Unlike MCF-7, SUM149PT cells do not require estrogen supplementation and are considered non-invasive upon orthotopic implantation.[9] Moreover, SUM149PT cells are negative for NKG2D–DAP10, thus precluding functional contributions from residual endogenous receptor expression (Figures 2b and c). We established SUM149PT transfectants stably expressing NKG2D–DAP10 (SUM149PT–TF) or empty vector (SUM149PT–mock) controls linked to a green-fluorescence protein (GFP) cassette (Figures 2b and c). NKG2D–DAP10 signaling proficiency was tested by antibody-mediated NKG2D crosslinking on desensitized cells

and probing of immunoblots for PI3K-dependent phosphorylation of AKT (P-AKT) at position S473. Similarly, triggering of NKG2D resulted in independent activation of P-ERK1/2 (T202/Y204) and P-JNK1/2 (T183/Y185) in MAPK signaling cascades. Responses were similar to those elicited by epidermal growth factor (EGF) (Figure 2d). Thus, as with other tumor lines and ex vivo cancer cells studied before, NKG2D–DAP10 activated the main oncogenic signaling axes in SUM149PT–TF but not in control SUM149PT cells.

After confirming stability of ectopic and negative control NKG2D phenotypes in a 7-week in vivo pilot experiment, groups
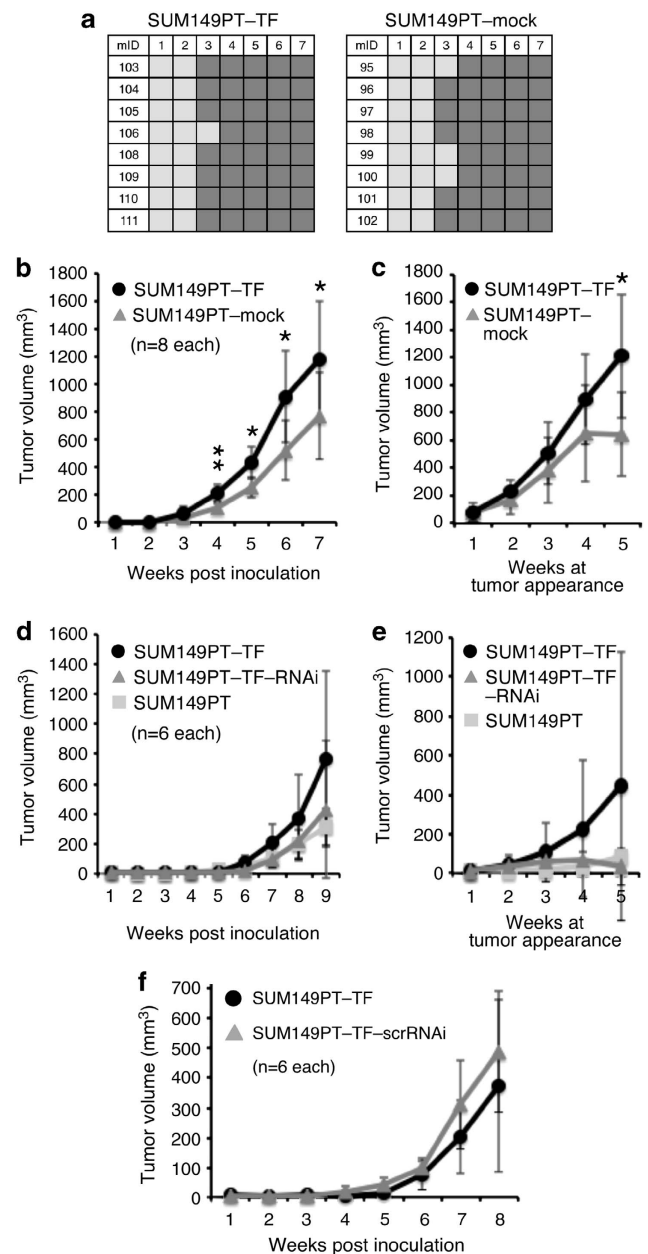
of each eight non-obese diabetic/severe combined immunodeficient mice received mammary fat pad injections of SUM149PT–TF or SUM149PT–mock cells, followed by weekly monitoring of tumor development and size. All mice were euthanized 7 weeks post inoculation as some tumors reached Institutional Review Board protocol-approved maximum limit size. At this stage, NKG2D phenotype stability was confirmed in all animals (Figure 2e). Operationally, this experiment will be referred to as 'run 1' from here on. Unlike the MCF-7 model, latency and tumor incidence were minimally affected by NKG2D–DAP10 at the 3-week interval and were similar between the experimental and control groups at week 4 (Figure 3a). SUM149PT–TF tumor growth versus negative control, however, was notably enhanced. Adjustment of tumor volumes for time of tumor appearance yielded similar outcomes (Figures 3b and c). Formal confirmation of NKG2D involvement in these effects was independently obtained using NKG2D-depleted SUM149PT–TF (SUM149PT–TF–RNAi) cells versus SUM149PT–TF and SUM149PT wild-type cells (Figures 3d and e; see Figure 2b for confirmation of NKG2D phenotypes). This experiment, referred to as 'run 2' from here on, corroborated the absence of NKG2D effects on tumor latency and incidence seen in run 1. Consistent with NKG2D-promoting tumor growth, SUM149PT–TF–RNAi tumor volumes, without or with adjustment for time of tumor appearance, were similar to those of SUM149PT wild-type tumors and smaller than those of SUM149PT–TF tumors (Figures 3d and e). Control SUM149PT–TF–scrRNAi-derived data corresponded to those derived from SUM149PT–TF cells (Figure 3f).
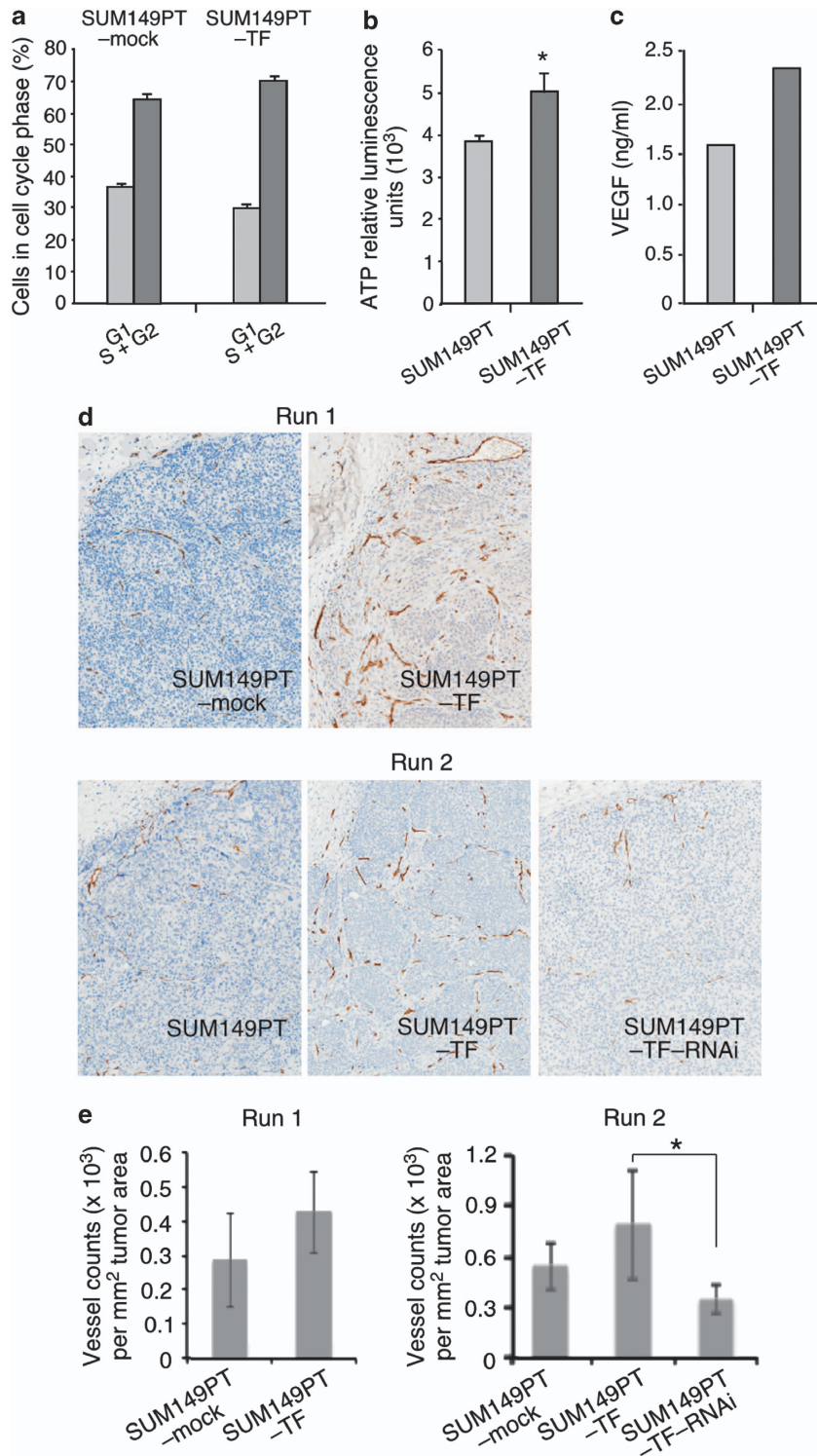
Cancer cell NKG2D may promote tumor-associated angiogenesis in vivo
Tumor growth is a function of determinants including cancer cell proliferation, survival and blood supply, or combinations thereof. In cell culture, ligand-mediated NKG2D self-stimulation

of MCF-7–TF, and to a lesser extent of SUM149PT–TF cells, enhanced cell cycle progression and ATP production (Figures 4a and b).[8] We thus tested each four run 1 SUM149PT–TF and negative control (SUM149PT–mock) tumors for the Ki-67 proliferation marker in immunohistochemistry stainings. Contrasting the in vitro observations, SUM149PT–TF cell proliferation appeared unaffected by NKG2D in vivo. By microscopic inspection, sections from both tumor groups were indistinguishable, showing multiple irregularly distributed areas in which most tumor cells stained positive for Ki-67. Histoquest (TissueGnostics, Vienna, Austria) software-supported morphometry of at least three such areas per tumor section indicated proliferation indices of ~85% in both groups (86.23 ± 7.67% versus 85.37 ± 5.89%). Analysis of each four SUM149PT–TF and control tumors from the run 2 experiment substantiated this phenotype. Cultured SUM149PT cells themselves already have a high baseline proliferation rate (Figures 4a and b). Relatively small differences in cellular functions measured in vitro may not become apparent in vivo because of masking by tissue environmental factors.

Figure 3. NKG2D effects on tumor latency, incidence and growth in the orthotopic SUM149PT xenotransplant model. (**a**) Graphic representation of tumor development over time measured in weekly intervals (top numbers) following implantation of SUM149PT–TF and SUM149PT–mock lines shows absence of NKG2D effects on tumor latency and frequency. Dark gray squares indicate the presence of measurable tumor mass; light gray squares indicate absence of tumor mass. Left vertical numbers refer to mID. (**b**) Graphic representations of SUM149PT–TF and SUM149PT–mock tumor volume averages and s.d.'s at the indicated weekly time intervals post inoculation. Data were derived from each eight mice per group corresponding to those in (**a**) monitored for 7 weeks. Asterisk denotes P < 0.05; double asterisk denotes P < 0.001. (**c**) Graphic representation of SUM149PT–TF and SUM149PT–mock tumor volume averages normalized to times of tumor appearance. Data were derived from the same mice studied in (**b**). Normalization of tumor volumes to times of tumor appearances affects group sizes at each weekly interval as follows: weeks 1–4, SUM149PT–TF (n = 8) and SUM149PT–mock (n = 8); week 5, SUM149PT–TF (n = 7) and SUM149PT–mock (n = 5). Asterisk denotes P < 0.05. (**d**) Graphic representations of SUM149PT–TF, SUM149PT–TF–RNAi and SUM149PT tumor volume averages and s.d.'s at the indicated weekly time intervals post inoculation. Data were derived from each six mice per group monitored for at least 9 weeks in experiment denoted run 2 (see text). (**e**) Graphic representation of SUM149PT–TF, SUM149PT–TF–RNAi and SUM149PT tumor volume averages normalized to times of tumor appearance. Data were derived from the same mice studied in (**d**). Normalization of tumor volumes to times of tumor appearances affects group sizes at each weekly interval as follows: weeks 1–4, SUM149PT–TF (n = 6), SUM149PT–TF–RNAi (n = 6) and SUM149PT (n = 6); week 5, SUM149PT–TF (n = 6), SUM149PT–TF–RNAi (n = 5) and SUM149PT (n = 6). (**f**) Representation of SUM149PT–TF and SUM149PT–TF–scrRNAi tumor volume averages and s.d.'s at the indicated weekly time intervals post-tumor cell inoculation. Data were derived from each six mice per group monitored for 8 weeks.

Figure 4. NKG2D promotes *in vitro* cellular functions and tumor-associated angiogenesis in the orthotopic SUM149PT xenotransplant model in separate experiments referred to as run 1 and run 2. (**a**) Cell cycle analysis of SUM149PT–TF and SUM149PT–mock cells by propidium iodide (PI) staining and quantitative evaluation of flow cytometry data based on Dean–Jett–Fox curve fitting. (**b**) Comparison of SUM149PT–TF and SUM149PT–mock cells for total cellular ATP. Asterisk denotes $P < 0.05$. Data shown are representative of three experiments. (**c**) Comparison of SUM149PT–TF and SUM149PT–mock cells for secretion of VEGF using ELISA. Data shown in are representative of three experiments. (**d**) Micrographs of tumor tissue sections stained for mouse endothelial CD31 show highly vascularized SUM149PT–TF tumor margins contrasting the poorly vascularized negative control SUM149PT–mock and SUM149PT tumors. RNAi-mediated NKG2D depletion in SUM149PT–TF–RNAi tumors reverts the SUM149PT–TF-associated vascularization phenotype. Upper left corners in each micrograph show areas of peritumoral stroma. Images are representative of each four tumors per experimental group and were derived from whole section TissueFAXS scans at a $\times 10$ magnification. (**e**) Graphic representation of vessel count means ± s.d.'s per mm^2 of tumor areas. Each four tumors were analyzed per experimental group. Vessel counts from each three fields per section were obtained using ImageJ software. Asterisk denotes $P < 0.05$.

6

By activating the PI3K–mammalian target of rapamycin and MAPK signaling axes, cancer cell NKG2D may also elicit survival responses affecting tumor growth.[10] Poly ADP-ribose polymerase (PARP) is a protein involved in DNA repair and programmed cell death. PARP is mainly activated by caspase-3-mediated cleavage in the apoptotic cascade and serves as a marker of cells undergoing apoptosis.[11] SUM149PT–TF and control sections from each four run 1 experiment tumors were stained for activated PARP (cleaved PARP), and the positive nuclei were enumerated by employing the Histoquest software. In both groups, cleaved PARP-positive nuclei were scarce (<1% of total nuclei count), with no significant differences between SUM149PT–TF tumors and controls ($0.522 \pm 0.10\%$ versus $0.6175 \pm 0.24\%$). Examination of run 2 tumors gave no different results.

With no evidence for NKG2D effects on in vivo tumor cell proliferation and survival, we addressed angiogenesis as a factor favoring tumor growth. This possibility was encouraged by data indicating that cultured SUM149PT–TF cells produce larger amounts of vascular endothelial growth factor (VEGF) as compared with SUM149PT–TF–mock and SUM149PT–TF–RNAi cells (Figure 4c). Tumor vascularization was examined by immunohistochemistry of endothelial CD31 in run 1 and run 2 experimental tumors using mouse-specific primary antibody. In contrast to control tumors, which were poorly vascularized throughout, those expressing NKG2D showed enhanced vascularization that was most evident within tumor margins (Figure 4d). Vessel counts performed with ImageJ (http://rsbweb.nih.gov/ij) corroborated the microscopic assessments (Figure 4e). Unlike in the run 1 experiment, in which all tumors were harvested at week 7 post implant and thus differed in size, run 2 experimental end points were controlled for tumor volume, thus emphasizing that the observed vascularization increase was in fact linked to NKG2D and not simply tumor volume-associated. Moreover, as with overall tumor growth, vessel counts from NKG2D-depleted SUM149PT–TF–RNAi tumors resembled those of wild-type controls, thus confirming a role of NKG2D in promoting tumor angiogenesis. Altogether, these results point to angiogenesis as a rate-limiting factor in NKG2D-mediated enhancement of tumor growth. As to in vivo VEGF plasma concentrations, however, results were inconclusive. Although VEGF concentrations in run 1 SUM149PT–TF mouse plasma samples were higher than those in control mice, those differences disappeared when values were normalized for tumor volumes. Similarly, no differences in plasma VEGF were found with the tumor volume-controlled run 2 mice. However, the absence of systemic VEGF increases does not preclude an NKG2D effect on local tumor microenvironmental VEGF supplies.

Cancer cell NKG2D enhances intravasation and distant metastasis seeding in vivo

During thorough inspections of CD31-stained SUM149PT–TF tumor sections, we occasionally noted peritumoral vessel lumina filled with groups of atypical cells resembling tumor cells. Staining of consecutive serial tissue sections for the human pan-cytokeratin AE1/AE3 tumor cell marker confirmed the human tumor cell identity of those cells, which presumably entered the vasculature via intravasation (Figure 5a). Such examples of tumor cell intravasation were rare and detected in only two of the eight run 1 and one of the six run 2 SUM149PT–TF tumor sections. However, none of the negative control tumor sections from both experiments showed any evidence of intravasation, even upon scrutiny of sections from three tumor levels separated by $50 \, \mu m$.

In addition to promoting tumor growth, NKG2D-enhanced vascularization may provide increased access of tumor cells to vasculature, thereby facilitating intravasation followed by tumor cell dissemination leading to distant metastasis. To examine

SUM149PT–TF and negative control-xenografted mice for evidence of metastatic tumor cell dissemination, explanted lungs were examined using GFP imaging employing scanning and fluorescence microscopy. Six of the eight run 1 SUM149PT–TF mouse model lungs displayed strong GFP signals compared with only two of the eight control lungs. Moreover, all the six run 2 SUM149PT–TF and SUM149PT–TF–scrRNAi mouse model lungs contained GFP-positive foci as opposed to only two of the six SUM149PT–TF–RNAi lungs (Figure 5b). Subsequent examination of serial lung sections that were alternatingly stained with hematoxylin/eosin (H&E) and for AE1/AE3 confirmed that GFP signals corresponded to occurrences of AE1/AE3-positive human tumor cells. All of three GFP-positive SUM149PT–TF mouse model lungs harbored numerous multicellular clusters of histopathologically atypical AE1/AE3-positive cells indicative of micrometastases (Figure 5c). Altogether, these results suggest that NKG2D may facilitate tumor metastasis at the level of accessibility of tumor cells to vasculature.

DISCUSSION

This study builds on findings suggesting a moonlighting role of the stimulatory NKG2D lymphocyte receptor as an oncoprotein in human cancer, functionally endowed by the concomitant presence of its ligands on cancer cells. This capacity is supported by NKG2D-mediated activation of the main oncogenic signaling pathways and resultant functional effects in vitro, as well as by correlative clinical studies.[8] However, evidence for pathophysiological significance of cancer cell NKG2D has remained incomplete as its tumorigenic capacity was untested in vivo. Using NKG2D–DAP10 transfectants of the MCF-7 and SUM149PT breast cancer lines and controls in classical orthotopic xenotransplant mouse models, we have now shown that NKG2D has tumor-promoting abilities, thus supporting the idea that cancer cells co-opt the expression of NKG2D to complement the presence of its ligands for oncogenic self-stimulation. Consequently, our results may have an impact on immunotherapy approaches, which currently do not account for such NKG2D effects in cancer patients and thus could be misdirected, as underlying assumptions are incomplete.[12–16]

Specifically, our study offers the main conclusions that NKG2D may promote tumor initiation, and tumor growth and dissemination by enhancing tumor-associated angiogenesis. These conclusions are derived from the MCF-7 and SUM149PT orthotopic xenograft experiments, which are established models to interrogate oncogenic effects and document stages and aspects of tumor progression that may be involved. The MCF-7-based model, initially chosen because of our previous in vitro studies of these cells, failed largely due to rapid loss of ectopic NKG2D expression on the MCF-7–TF cells in mice. Nevertheless, however, these experiments revealed a pronounced association between NKG2D and reduced latency and increased tumor take. Hence, MCF-7–TF cells may have been reprogrammed for increased tumor-initiating abilities. Tumor initiation by MCF-7 cells may be regulated by estrogen receptor signaling.[17] Preliminary data indicate diminished estrogen receptor expression in MCF-7–TF as opposed to control cells, hence raising the possibility that the enhanced tumorigenicity of MCF-7–TF cells may be accounted for by reduced estrogen dependence. In addition or alternatively, NKG2D signals in MCF-7–TF cells might act at a level of transcriptional cancer stem cell reprogramming.

Insights gained from the SUM149PT-based xenograft model were different but complementary. Tumor initiation by SUM149PT–TF cells was not noticeably affected by NKG2D, possibly because of the highly tumorigenic attributes of the parent cells masking more subtle effects. Tumor growth, on the other hand, was significantly enhanced by NKG2D, which was substantiated by RNAi-mediated NKG2D silencing. However, despite its activation of the signaling
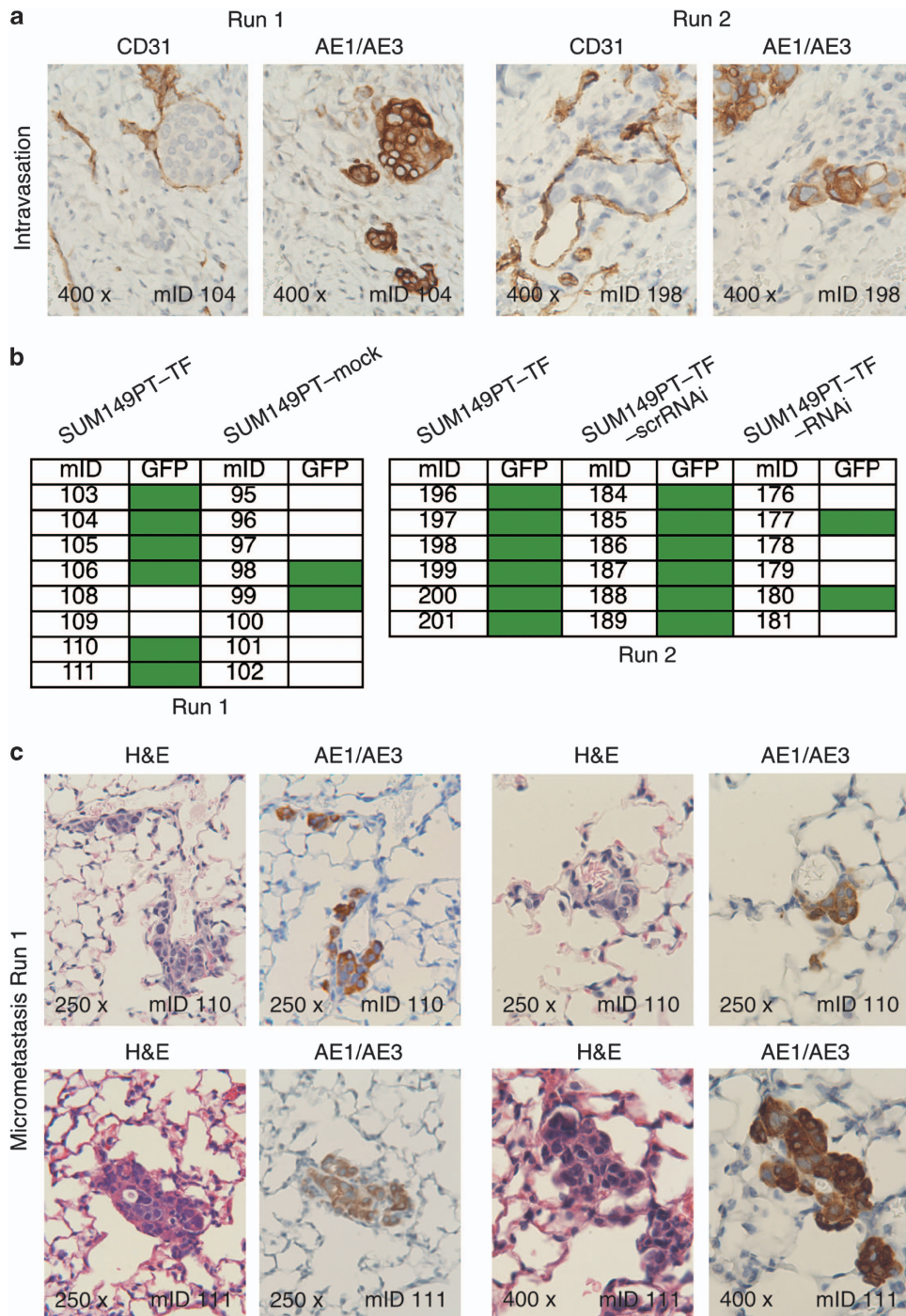
Figure 5. NKG2D enhances intravasation and micrometastasis in the orthotopic SUM149PT xenotransplant model. (**a**) Two micrograph pairs of SUM149PT–TF serial tumor tissue sections stained for mouse endothelial CD31 or human pan-cytokeratin AE1/AE3 as human tumor cell marker. Micrograph pairs were derived from run 1 and run 2 experiments and document examples of human tumor cells located within cross-sections of CD31-positive peritumoral vessels. (**b**) Schematic representation of the presence of absence of GFP signals in lungs explanted from the run 1 and run 2 experimental and control hosts. Green boxes represent positive GFP signals revealed by Typhoon Trio scanning. (**c**) Four micrograph pairs of serial lung tissue sections from run 1 SUM149PT–TF tumor hosts stained for H&E or human pan-cytokeratin AE1/AE3. Each of the two micrograph pairs were derived from two different mice and show examples of micrometastasic clusters of AE1/AE3-positive cells. Numbers in bottom left micrograph corners indicate microscopic magnification; numbers in bottom right micrograph corners specify mIDs.

pathways known to promote tumor cell proliferation and survival, none of these parameters appeared to have contributory effects. Instead, we found that NKG2D acted at the level of tumor-associated angiogenesis, another determinant driving tumor growth that can be regulated by PI3K–mammalian target of

rapamycin and MAPK signals.[18] Tentatively, increased tumor cell access to vasculature may account for our other observation of increased tumor-cell dissemination to distant sites seen in NKG2D positive as opposed to negative tumor hosts. This model is consistent with trend associations, and significant positive

correlations, between frequencies of NKG2D-positive cells in human cancers and extents of lymphovascular invasion, and lymph node involvement, respectively.[8]

In summary, our mouse model studies indicate a role of cancer cell NKG2D as a driver of *in vivo* tumor development and progression. Effects of NKG2D on components of tumorigenesis may depend on cell intrinsic properties and thus vary among different cell line model systems. Notwithstanding this possibility, however, our results expand current knowledge of the conflicting roles of this receptor at the dynamic interface between the immune system and cancer biology.

MATERIALS AND METHODS

Tumor lines
Transfectants of the MCF-7 breast cancer line (American Type Culture Collection) with ectopic expression of NKG2D–DAP10 (MCF-7-TF), mock-transfected controls (MCF-7–mock), MCF-7–TF cells with RNAi-induced NKG2D depletion (MCF-7-TF–RNAi), MF7-7 wild-type cells with RNAi-induced NKG2D depletion (MCF-7–RNAi) and scrambled (scr) RNAi controls (MCF-7-TF–scrRNAi and MCF-7–scrRNAi) have been described.[8] MCF-7 and descendent lines were maintained in RPMI-1640/10% fetal bovine serum/antibiotics. Transfectants of the SUM149PT (Asterand, Detroit, MI, USA) breast cancer line (SUM149PT–TF and SUM149PT–mock) were established using vectors with a GFP cassette as described, as was lentiviral transduction of SUM149PT–TF cells with NKG2D RNAi or scrRNAi (SUM149PT–TF–RNAi and SUM149PT–TF–scrRNAi).[8] These cells were maintained following the online recommendation at www.Asterand.com.

Immunoprecipitations and immunoblots
NKG2D was immunoprecipitated from standard NP-40 buffer lysates of SUM149PT ($\sim 5 \times 10^7$) and SUM149PT–TF cells (5×10^6) using monoclonal antibody (mAb) 5C6 immobilized on AminoLink Plus Coupling Resin (Pierce, Rockford, IL, USA).[8] Immunoblots were probed with polyclonal antibodies to NKG2D or DAP10 (N-20 and N-17; Santa Cruz Biotechnology, Santa Cruz, CA, USA) and developed using secondary reagents and Supersignal West Dura Extended Duration Substrate (Pierce). For *P*-AKT induction, tumor cells (2×10^6 per experimental condition) cultured in six-well plates were desensitized for 16 h in serum-free RPMI at 37 °C before exposure in 0.5 ml RPMI to EGF (rhEGF, 100 ng/ml; Sigma, St Louis, MO, USA; 10–20 min at 37 °C), mAb 1D11 (purified with MabTrap Kit; GE Healthcare Life Sciences (Pittsburgh, PA, USA); 5 µg/ml, 30 min at 4 °C). For crosslinking, washed cells in 0.2 ml RPMI were exposed to goat anti-mouse F(ab')₂ (20 µg/ml; 5 min at 37 °C; Jackson ImmunoResearch, West Grove, PA, USA). LY294002 (100 nM; Sigma) was applied 2 h before stimulations. Reactions were terminated on ice by addition of 1 ml sodium orthovanadate (Na₃VO₄, 2 mM in cold phosphate-buffered saline (PBS); Calbiochem, San Diego, CA, USA) and cells resuspended in NP-40 lysis buffer with protease inhibitor cocktail (Roche, Indianapolis, IN, USA) and Na₃VO₄. Cleared supernatants were subjected to SDS–PAGE (4–12% gradient NuPAGE gels; Invitrogen, Carlsbad, CA, USA) and proteins were electroblotted onto polyvinylidene fluoride membranes (Immobilon-P; Millipore, Billerica, MA, USA), which were probed with rabbit anti-human phospho-AKT(S473) (clone 193H12) or pan-AKT (clone C67E7), secondary horseradish peroxidase-conjugated anti-rabbit IgG (all from Cell Signaling Technology, Danvers, MA, USA) and chemiluminescent reagent. MAPKs were detected with cells grown to semi-confluence in six-well plates and desensitized for 24 h. PI3K inhibitor LY294002 (100 nM) or inhibitors of MEK/ERK (U0126, 10 µM; Cell Signaling Technology) or JNK (SP600125, 100 µM; Sigma) were added 30 min before stimulations. EGF (rhEGF, 100 ng/ml; Sigma) was added for 10–20 min at 37 °C. NKG2D was crosslinked and the samples were processed as above, run in 4–12% gradient NuPAGE gels and immunoblots were probed using rabbit mAb to *P*-p44/42 MAPK (ERK1/2(T202/Y204)) and *P*-SAPK/JNK(T183/Y185) (clones 137F5 and 81E11) (all from Cell Signaling Technology).

Surgery, necropsy, tissue processing and GFP imaging
All animal procedures were approved by the FHCRC Institutional Review Board (IACUC no. 1870). Six- to eight-week-old female non-obese diabetic/severe combined immunodeficient mice were obtained from the FHCRC Core Center of Excellence in Hematology (DK-56465) and housed under pathogen-free conditions at the FHCRC Comparative Medicine Shared

Resource. Recipients of MCF-7 cells were supplemented with 60-day release 17β-Estradiol pellets (0.72 mg; Innovative Research of America, Sarasota, FL, USA) 1 week prior to tumor line implant.[19,20] For the implants, mice were anaesthetized with isoflurane, subjected to small skin incisions exposing the second mammary fat pad and orthotopically injected with MCF-7 (5×10^6 viable cells) or SUM149PT (2×10^6 viable cells) derivative cells or controls in 50 µl growth medium (1:1 PBS/BD Matrigel Matrix; BD Biosciences, Bedford, MA, USA). Wound closure was with sutures. Tumor development and growth was monitored weekly by external vernier caliper (VWR, Radnor, PA, USA). Tumor volume was calculated as $V = 4/3 \times \pi \times (L/2 \times W/2 \times W/2)$, with L = length and W = width. At experimental end points or when a tumor parameter reached 1.5 cm, whichever came first, animals were euthanized. Blood was harvested by cardiac puncture and plasma-prepared using centrifugation. Primary tumors were resected, weighed and processed for flow cytometry, routine H&E histology and immunohistochemistry. Lungs were perfused with PBS, resected and subjected to GFP imaging using a Typhoon Trio scanner at the excitation of 488 nm and were detected through a 500–540 bypass filter. Lobes with single-positive GFP signals where subsequently imaged using a Nikon TI fluorescent microscope with a PlanApo × 2/0.1 objective. Following GFP imaging, lungs were fixed in 10% neutral-buffered formalin.

Flow cytometry and immunohistochemistry
Tumor specimens were processed to single-cell suspensions as described,[21] or by using a human Tumor Tissue Dissociation Kit and gentleMACS Dissociator (both from Miltenyi Biotech, Bergisch Gladbach, Germany). Tumor cell suspensions were treated with PBS/10% human serum/0.15% sodium azide for 15 min at room temperature, followed by incubation with pretitrated mAb-fluorochrome conjugates to NKG2D (clone 1D11; 2), MICA/B (clone 6D4; 2), ULBP1 (clone 170818; R&D Systems, Minneapolis, MN, USA), ULBP2 (clone 165903; R&D Systems), ULBP3 (clone 166510; R&D Systems), ULBP4 (1H11; 8) and ULBP5 (clone 8C10; 8) for 30 min on ice, followed by a wash in PBS/4',6-diamidino-2-phenylindole for live/dead cell distinction. Isotype-specific Ig were used as controls. Stained cell suspensions were analyzed using a BD LSR II flow cytometer (BD Biosciences) and FlowJo software (Tree Star, Ashland, OR, USA). Histology and immunohistochemistry were performed using the FHCRC Experimental Histopathology Shared Resource. Formalin-fixed tissues were paraffin-embedded, sectioned and stained with H&E or subjected to heat-induced epitope retrieval for subsequent immunohistochemistry using a Dako Cytomation Autostainer. Blocking of endogenous peroxidase was with 3% H₂O₂. Unspecific antibody-binding block used TCT buffer (Tris-OH (0.05 M, pH 7.6)/NaCl (0.15 M)/Casein (0.25%)/Tween-20 (0.1%)) and additional goat (15%) and mouse (15%) serum for CD31 immunohistochemistry. Primary antibodies included anti-human pan-cytokeratin (mAb AE1/AE3; Dako, Carpinteria, CA, USA), anti-human Ki-67 mAb (clone MIB-1; Dako), human-specific anti-Cleaved PARP (Asp214; Cell Signaling) and anti-mouse CD31 (PECAM-1) mAb (clone SZ31; Dianova, Hamburg, Germany). Isotype Ig was used as controls. Mouse on mouse detection used rabbit anti-mouse Fab (Jackson ImmunoResearch), normal mouse serum and MACH2 rabbit HRP polymer (Biocare Medical, Concord, CA, USA). Rat horseradish peroxidase polymer (Biocare Medical) was used together with rat anti-mouse CD31. Antibody/horseradish peroxidase polymer binding was visualized with 3,3'-diaminobenzidine (Dako) substrate. Counterstaining was with hematoxylin (Dako). Sections were examined using Nikon Eclipse 800 (Nikon Instruments, Melville, NY, USA) or Leitz Laborlux S microscopes and the Leica Application Suite (both from Leica Mikrosysteme, Wetzlar, Germany). Morphometry employed a TissueFAXS (TissueGnostics, Vienna, Austria) digital pathology system with a × 10/0.3 NA objective for slide scanning and proprietary HistoQuest (TissueGnostics) and public domain ImageJ software for morphometric analysis. HistoQuest was used to count positive and negative nuclei based on color segmentation of blue versus brown cells. ImageJ was used to count vessels by thresholding the image for light staining (total tissue) or dark staining (vessels), and by using the particle analysis tool. Ki-67 and cleaved PARP morphometry was standardized to involve at least three (pre-selected for high ratios of positive to negative nuclei) areas per tumor section. This approach was necessary to control for the irregular distribution of positive signals for both markers in all tumors. Similarly, CD31 morphometry compared areas of highest CD31 signal densities in each experimental group. To screen for the presence of xenotransplant cells disseminated into the lungs, each fifth section in series of 100 consecutive sections per tissue block was H&E-stained and examined for histopathological criteria suggestive of micrometastases followed

by confirmatory AE1/AE3 immunohistochemistry of consecutive serial sections.

Cell cycle analysis, and ATP and VEGF assays

Cell cycle analysis based on determinations of DNA content was performed as described.[8] Cellular ATP was quantified using the ATPlite luminescence assay system (PerkinElmer, Waltham, MA, USA). VEGF in cell culture supernatants and mouse plasma was measured using Luminex multiplex assay. Luminex microbeads coated with anti-human VEGF mAb (clone 26503; R&D Systems) were sequentially incubated in plasma samples, biotinylated polyclonal goat anti-mouse detection antibody (R&D Systems) and fluorescently tagged streptavidin conjugate, with washes in between. Assays were read on a Luminex 200 instrument (Luminex Corp., Austin, TX, USA), with fluorescence directly proportional to sample VEGF concentrations as deduced from standard curve.

Statistical analysis

The mean tumor volumes at specific time points were compared between groups using the two-sample *t*-test. Specific time points were defined from inoculation as well as from first appearance of tumor. Tumor growth curves were compared between groups using the two-sample test by calculating the average tumor volume for each animal and then comparing the means of these average volumes.

CONFLICT OF INTEREST

The authors declare no conflict of interest.

REFERENCES

1 Nausch N, Cerwenka A. NKG2D ligands in tumor immunity. *Oncogene* 2008; **27**: 5944–5958.

2 Bauer S, Groh V, Wu J, Steinle A, Phillips JH, Lanier LL *et al.* Activation of NK cells and T cells by NKG2D, a receptor for stress-inducible MICA. *Science* 1999; **285**: 727–729.

3 Lanier LL. Up on the tightrope: natural killer cell activation and inhibition. *Nat Immunol* 2008; **9**: 495–502.

4 Upshaw JL, Leibson PJ. NKG2D-mediated activation of cytotoxic lymphocytes: unique signaling pathways and distinct functional outcomes. *Semin Immunol* 2006; **18**: 167–175.

5 Gonzalez S, Groh V, Spies T. Immunobiology of human NKG2D and its ligands. *Curr Top Microbiol Immunol* 2006; **298**: 121–138.

6 Eagle RA, Trowsdale J. Promiscuity and the single receptor: NKG2D. *Nat Rev Immunol* 2007; **7**: 737–744.

7 Raulet DH, Gasser S, Gowen BG, Deng W, Jung H. Regulation of ligands for the NKG2D activating receptor. *Annu Rev Immunol* 2013; **31**: 413–441.

8 Benitez AC, Dai Z, Mann HH, Reeves RS, Margineantu DH, Gooley TA *et al.* Expression, signaling proficiency, and stimulatory function of the NKG2D lymphocyte receptor in human cancer cells. *Proc Natl Acad Sci USA* 2011; **108**: 4081–4086.

9 Ma L, Young J, Prabhala H, Pan E, Mestdagh P, Muth D *et al.* miR-9, a MYC/MYCN-activated microRNA, regulates E-cadherin and cancer metastasis. *Nat Cell Biol* 2010; **12**: 247–256.

10 Kooijman R. Regulation of apoptosis by insulin-like growth factor (IGF)-1. *Cytokine Growth Factor Rev* 2006; **17**: 305–323.

11 Kaufman SH, Desnoyers S, Ottaviano Y, Davidson NE, Poirier GG. Specific proteolytic cleavage of poly (ADP-ribose) polymerase: an early marker of chemotherapy-induced apoptosis. *Cancer Res* 1993; **53**: 3976–3985.

12 von Strandmann EP, Hansen HP, Reiners KS, Schnell R, Borchmann P, Merkert S *et al.* A novel bispecific protein (ULBP2-BB4) targeting the NKG2D receptor on natural killer (NK) cells and CD138 activates NK cells and has potent antitumor activity against human multiple myeloma in vitro and in vivo. *Blood* 2006; **107**: 1955–1962.

13 Cho HM, Rosenblatt JD, Tolba K, Shin SJ, Shin DS, Calfa C *et al.* Delivery of NKG2D ligand using an anti-HER2 antibody-NKG2D ligand fusion protein results in an enhanced innate and adaptive antitumor response. *Cancer Res* 2010; **70**: 10121–10130.

14 Zhang T, Sentman CL. Cancer immunotherapy using a bispecific NK receptor fusion protein that engages both T cells and tumor cells. *Cancer Res* 2011; **71**: 2066–2076.

15 Lehner M, Gotz G, Proff J, Schaft N, Dorrie J, Full F *et al.* Redirecting T cells to Ewing's sarcoma family of tumors by a chimeric NKG2D receptor expressed by lentiviral transduction or mRNA transfection. *PLoS One* 2012; **7**: e31210.

16 Song DG, Ye Q, Santoro S, Fang C, Best A, Powell DJ *et al.* Chimeric NKG2D CAR-expressing T cell-mediated attack of human ovarian cancer Is enhanced by histone deacetylase Inhibition. *Hum Gene Ther* 2013; **24**: 295–305.

17 Noel A, Simon N, Raus J, Foidart JM. Basement membrane components (matrigel) promote the tumorigenicity of human breast adenocarcinoma MCF7 cells and provide an in vivo model to assess the responsiveness of cells to estrogen. *Biochem Pharmacol* 1992; **43**: 1263–1267.

18 Jiang B-H, Liu L-Z. PI3K/PTEN signaling in angiogenesis and tumorigenesis. *Adv Cancer Res* 2009; **102**: 19–65.

19 Yang J, Bielenberg DR, Rodig SJ, Doiron R, Clifton MC, Kung AL *et al.* Lipocalin 2 promotes breast cancer progression. *Proc Natl Acad Sci USA* 2009; **106**: 3913–3918.

20 Ben-Batalla I, Seoane S, Garcia-Caballero T, Gallego R, Macia M, Gonzalez LO *et al.* Deregulation of the Pit-1 transcription factor in human breast cancer cells promotes tumor growth and metastasis. *J Clin Invest* 2010; **120**: 4289–4302.

21 Groh V, Rhinehart R, Secrist H, Bauer S, Grabstein KH, Spies T. Broad tumor-associated expression and recognition by tumor-derived gamma delta T cells of MICA and MICB. *Proc Natl Acad Sci USA* 1999; **96**: 6879–6884.